nature neuroscience

Temporal integration by calcium dynamics in a model neuron

Yonatan Loewenstein & Haim Sompolinsky

The calculation and memory of position variables by temporal integration of velocity signals is essential for posture, the vestibulo-ocular reflex (VOR) and navigation. Integrator neurons exhibit persistent firing at multiple rates, which represent the values of memorized position variables. A widespread hypothesis is that temporal integration is the outcome of reverberating feedback loops within recurrent networks, but this hypothesis has not been proven experimentally. Here we present a single-cell model of a neural integrator. The nonlinear dynamics of calcium gives rise to propagating calcium wave-fronts along dendritic processes. The wave-front velocity is modulated by synaptic inputs such that the front location covaries with the temporal sum of its previous inputs. Calcium-dependent currents convert this information into concomitant persistent firing. Calcium dynamics in single neurons could thus be the physiological basis of the graded persistent activity and temporal integration observed in neurons during analog memory tasks.

Neurons in several brain areas show sustained spiking activity following a transient stimulus, with firing levels that vary with the stimulus parameters in a graded manner[1–4]. In some areas, the sustained firing rates are proportional to the time integral of the previous stimuli, making them candidate neuronal integrators[5,6]. A much-studied example is the oculomotor neural integrator. In the absence of external signals, the maintained firing rates of the integrator neurons produce signals that are used to maintain stable eye positions. Transient velocity signals change the level of the firing rate, enabling the system to generate the required eye movement to the newly encoded position[5,6]. It is not clear how this graded persistent activity is generated, primarily because the firing rate of these neurons is sustained for many seconds even in the absence of input from outside the integrator, whereas the time constant of their membrane potential response to current injection is in the milliseconds range[6]. Therefore, it has been suggested that the multiple states of persistent activity in neuronal integrators are the outcome of reverberating feedback loops within special recurrent networks[7–13].

The goldfish oculomotor integrator, however, shows seconds-long persistent activity even after extensive disruption of the integrator circuit[14]. Furthermore, no recurrent collateral axons have been found in the goldfish integrator nuclei. In addition, in the majority of the cells recorded, the amplitude of the membrane fluctuations, which presumably originate from excitatory postsynaptic potentials (EPSPs), was independent of their firing rate (which corresponds to the eye position)[6]. This suggests that, at least in these cells, the EPSPs do not originate from recurrent synapses. Moreover, recent theoretical studies suggest that finely graded persistent activity requires a large number of cells[12,13], whereas the number of neurons in the goldfish oculomotor neuronal integrator does not exceed 40 (ref. 14).

Very recently, graded persistent activity has been observed in single neurons in slices of the entorhinal cortex[15]. Although the required *in vitro* stimuli were unnaturally long, this has been proposed as a single-neuron mechanism that could subserve working memory. These results motivate the search for alternative, single-neuron mechanisms for graded persistent activity and integration. Such a mechanism requires the sustained firing rate of the neuron to be proportional to the integral over time of its previous synaptic inputs. The time constant of the membrane potential of neurons in the goldfish oculomotor neuronal integrator is short, as indicated by its fast response to pulse current injections[6]. This suggests that the sustained firing rate of the cell reflects the value of a dynamic variable other than the membrane potential that memorizes the integral of synaptic inputs but not that of current injections.

Calcium concentration is a plausible candidate for such a variable. Intracellular calcium dynamics generate rich spatiotemporal patterns, including oscillations[16,17] and propagating waves[18,19]. Of particular interest to us are calcium wave-fronts, which have been observed in several cell types[20–23], including neurons[24,25]. These phenomena result from regenerative calcium dynamics that involves the release of calcium from internal stores into the cytoplasm. This release is gated by various channels whose principal activator is the cytoplasmic calcium concentration ($[Ca^{2+}]_i$) itself. Thus, increasing $[Ca^{2+}]_i$ facilitates further release of calcium from the stores[17], a positive-feedback cycle known as calcium-induced calcium release (CICR).

Here we report that calcium wave-fronts within single neurons can generate graded persistent activity and temporally integrate incoming inputs. The diffusion of calcium together with its nonlinear autocatalytic dynamics give rise to wave-fronts of high calcium concentrations along dendritic processes of our model neuron. These fronts

Racah Institute of Physics, and Center for Neural Computation, Hebrew University, Jerusalem 91904, Israel. Correspondence should be addressed to Y.L. (ljonathan@fiz.huji.ac.il).

Published online 24 August 2003; doi:10.1038/nn1109

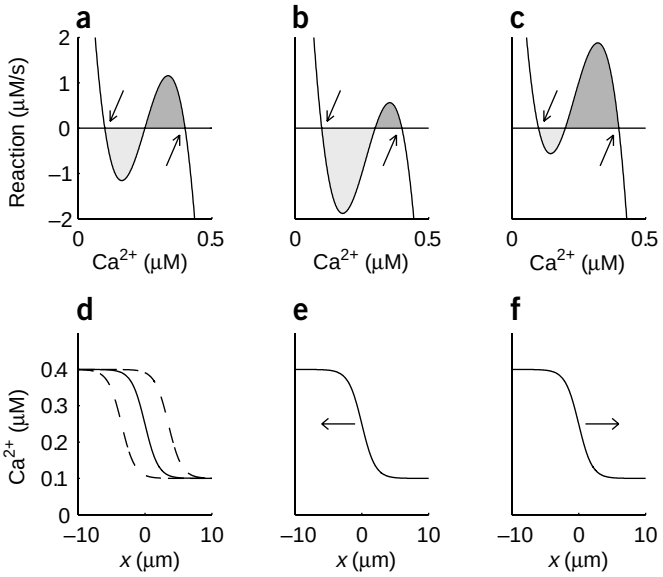

Figure 1 The generation of a $[Ca^{2+}]_i$ front. (**a**–**c**) Three examples of a $[Ca^{2+}]_i$ reaction function $f(c)$ (see equation (1) in Methods). The zero crossings of $f(c)$ correspond to the fixed points of the local dynamics in a small dendritic compartment. The functions in **a**–**c** all have the same stable fixed-points, corresponding to the same low and high $[Ca^{2+}]_i$ states (left arrow; $c = c_1 =$ 0.1 μM; right arrow; $c = c_3 = 0.4$ μM), but differ in the value of the intermediate unstable fixed point, c_2. The values of c_2 is 0.25 μM (**a**); 0.3 μM (**b**); 0.2 μM (**c**). (**d**–**f**) $[Ca^{2+}]_i$ along a dendrite. If $[Ca^{2+}]_i$ in the right and left ends of the dendrite are kept in the low and high $[Ca^{2+}]_i$ states, respectively, the $[Ca^{2+}]_i$ profile along the dendrite is a front (equation (3) in Methods). (**d**) If the areas of the negative (light gray) and positive (dark gray) parts of the reaction function are equal as in **a**, the front remains stationary at any location along the dendrite, illustrated here by two additional stationary fronts (dashed lines). (**e**) If the negative part is larger than the positive one as in **b**, the front will move to the left, increasing the region of low $[Ca^{2+}]_i$. (**f**) Conversely, if the positive part is smaller, as in **c**, the front will move to the right.

propagate at a speed that is proportional to the synaptic input to the cell, resulting in instantaneous front locations that vary in proportion to the temporal integration over previous inputs. Calcium-dependent currents translate the location of the fronts into concomitant persistent spiking activity. We show that integration by calcium dendritic dynamics can be considerably robust, due to the underlying nonlinearity and granularity of the dendritic calcium dynamics and the summation of signals from multiple dendritic branches.

RESULTS

The generation of calcium fronts

It has been suggested that calcium fronts are the outcome of the combined effect of the nonlinear CICR dynamics and diffusion[26]. We used a simple phenomenological model for the CICR mechanism. The rate of change of $[Ca^{2+}]_i$ in a small dendritic compartment is described by an N-shape reaction function, which includes the combined effects of uptakes of calcium from the cytoplasm by pumps and leakage through the membrane, as well as the nonlinear receptor-mediated release from the stores (equation (1) in Methods; **Fig. 1a–c**). In an appropriate range of parameters, this function gives rise to two stable states: low and high $[Ca^{2+}]_i$. When $[Ca^{2+}]_i$ is low, the calcium channels in the stores are closed, resulting in a stable low $[Ca^{2+}]_i$ state. Conversely, if $[Ca^{2+}]_i$ exceeds a threshold (the middle zero crossing of the reaction function), it triggers the release of calcium from internal stores, which leads to a high $[Ca^{2+}]_i$ steady state[26,27]. In a long dendritic branch, this local bistability of the calcium dynamics may give rise to a spatial profile of $[Ca^{2+}]_i$ that depends on the concentrations at the ends of the dendritic branch. In our model, the $[Ca^{2+}]_i$ level at one end of the dendrite is kept in the low $[Ca^{2+}]_i$ state, whereas the other end is in the high $[Ca^{2+}]_i$ state (**Fig. 1d–f**). In this case, the solution of the reaction-diffusion equation of $[Ca^{2+}]_i$ along the dendritic branch (equation (2) in Methods) is a profile of $[Ca^{2+}]_i$ in the form of a front, which connects the region of the branch in the low $[Ca^{2+}]_i$ state with the region in the high $[Ca^{2+}]_i$ state (equation (3) in Methods). This profile can be either stationary (**Fig. 1d**) or moving (**Fig. 1e,f**), depending on the properties of the reaction function. The area under the positive part of the function drives the dynamics toward increasing values of $[Ca^{2+}]_i$. Similarly, the negative part of the function drives the dynamics toward decreasing values of $[Ca^{2+}]_i$. If the two areas are equal (**Fig. 1a**), there is no net force acting on the front, and it remains stationary. This stationary front can be stably located anywhere along the bulk of the dendrite (**Fig. 1d**). The multiplicity of stable front positions enables the dendrite to function as a sustained memory of an analog parameter. If the negative area is larger than the positive one (**Fig. 1b**), the low $[Ca^{2+}]_i$ state is more attractive. In this case, the solution of the reaction-diffusion equations is a front that propagates to the high $[Ca^{2+}]_i$ end of the dendritic branch, thereby increasing the region of the dendrite with a low $[Ca^{2+}]_i$ level (**Fig. 1e**). The converse holds for a negative bias in these areas (**Fig. 1c,f**).

Synaptic inputs, in particular the activation of metabotropic glutamatergic receptors (mGluRs), can modulate the release of calcium from the stores[19,28]. This will affect the calcium profile along the dendrite. For example, a decrease in the rate of calcium release from the internal stores will increase the negative area under the reaction function (**Fig. 1b**), thereby causing a previously stationary front to propagate toward the high $[Ca^{2+}]_i$ end of the dendrite, which will increase the region of the dendrite with a low $[Ca^{2+}]_i$ level (as in **Fig. 1e**). Conversely, an increase in the rate of calcium release will cause the front to propagate in the opposite direction (as in **Fig. 1f**). We modeled the effect of synaptic input by incorporating an input-dependent bias in the reaction function. In this way, the synaptic input controls both the direction and the speed of the propagation of the $[Ca^{2+}]_i$ front. When the dendritic branch receives time-varying, spatially homogeneous synaptic input, the front moves with a velocity that is proportional to the strength of the instantaneous input, and therefore the location of the front is proportional to an integral over time of the input (equation (5) in Methods). This is illustrated in **Fig. 2**, where a dendritic branch receives synaptic pulses of varying strength and duration (**Fig. 2a**). Each burst shifts the front so that its location accurately encodes the time integral of the input (**Fig. 2b,c**). In the context of the oculomotor integrator, the input pulses represent burst-like saccadic commands, and the location of the front represents the eye position[5,6]. Note that although the synaptic input is homogeneous along the entire dendritic branch, it affects the location but not the shape of the front along the dendrite (**Fig. 2d**).

Readout mechanism

Ultimately, information stored in the $[Ca^{2+}]_i$ signals must be decoded by the membrane potential at the axon hillock and communicated by action potentials. $[Ca^{2+}]_i$ influences the membrane potential through a variety of calcium-dependent hyperpolarizing and depolarizing conductances. Specifically, a muscarinic-activated, calcium-sensitive nonspecific cationic current has been shown to be

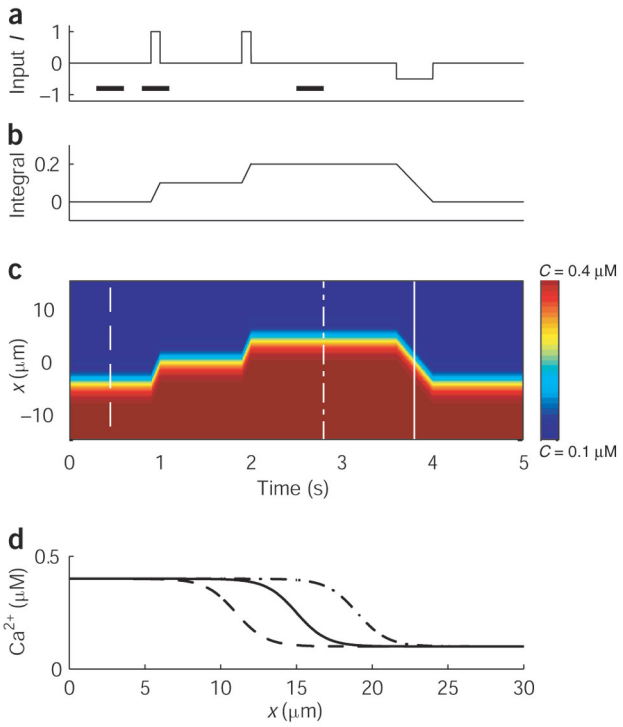

Figure 2 The effect of homogeneous synaptic input on the calcium front (equation (5) in Methods). (**a**) The stimulus consists of two spatially homogeneous positive pulses and one negative pulse, of widths 100 ms and 400 ms, respectively. The black bars correspond to **Fig. 4a–c**. (**b**) The integral over time of the input. (**c**) The local $[Ca^{2+}]_i$ along the dendrite (color coded) as a function of time. Color scale at right ranges from blue (c = 0.1 μM) to red (c = 0.4 μM). Note that the location of the front follows the temporal integral of the input (compare to **b**). (**d**) The shape of the front is independent of the location and of the input. The three fronts (dashed, solid and dash-dot) are sampled at three different points in time, denoted by white lines in **c** above.

essential for graded persistent activity in entorhinal cortex neurons[15]. In our model, we incorporated a calcium-dependent cationic current into a spiking neuron model (**Fig. 3a**). The calcium-dependent cationic channels are open solely in regions of the dendrite where $[Ca^{2+}]_i$ is high (red in **Fig. 3a**). Consequently, the total amount of depolarizing current (number of arrows in **Fig. 3a**) depends on the location of the $[Ca^{2+}]_i$ front along the dendrite. Below we discuss a more biologically plausible model, where the neuron is composed of many dendritic branches.

According to studies of integrator neurons *in vitro*, the relationship between firing rate and applied current is approximately linear, over a large range of input currents[29,30]. Therefore, we incorporated the calcium-dependent, nonspecific cationic current in a spiking neuron model in which the firing rate increases approximately linearly with the injected current above a threshold value[31] (see **Supplementary Methods** online). The firing rate as a function of the front location is illustrated in **Fig. 3b**. When the front is located at the extreme left end of the dendrite, the amount of calcium-dependent conductance is small and the cell does not fire. However, beyond a threshold of 5 μm from the tip of the dendrite, the firing rate is almost linear with the location of the front.

This model cell can accurately integrate incoming inputs. This is illustrated in **Fig. 4**, where the cell receives synaptic pulses of varying strength and duration as in **Fig. 2a**. The membrane potential at three different time intervals (denoted by black bars in **Fig. 2a**) is depicted in **Fig. 4a–c**. In the absence of input, the firing rate persists at a constant rate, reflecting the constant value of the integral (**Fig. 4a**). With the onset of positive external input, the firing rate increases (**Fig. 4b**), and when this input is terminated, the new firing rate persists at a new level, which corresponds to the new value of the integral (**Fig. 4c**). During this whole time, the instantaneous firing rate (line in **Fig. 4d**) is proportional to the time integral of the input (circles in **Fig. 4d**).

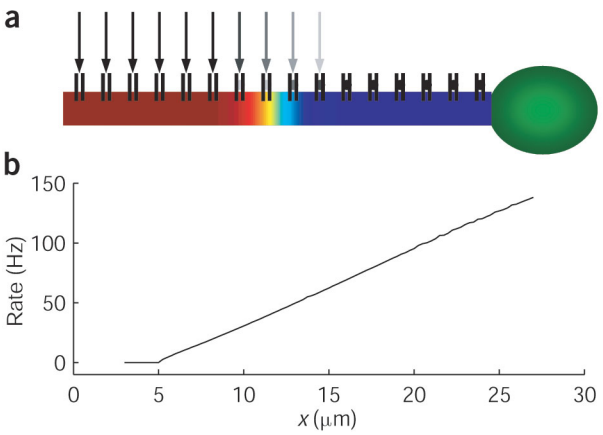

The effect of granularity

Real dendrites possess a considerable degree of spatial granularity, both in the sites of the synaptic inputs as well as in the locations of the intracellular calcium-secreting organelles. To test the consequences of this granularity, we simulated the propagation speed of $[Ca^{2+}]_i$ fronts in a chain of discrete calcium compartments (equation (7) in Methods). As shown in **Fig. 5**, the basic features of memory and integration are robust to the loss of spatial uniformity. The main effect of system granularity is the presence of an input threshold[26,32], below which the front does not move (arrow). Although such a threshold may lead to some loss of information, it endows the system with important resilience to weak distracting stimuli, a property which is known to be present in working-memory systems[4]. The granularity also yields a considerable robustness of the system to changes in the reaction function. In particular, a perturbation in the reaction function that yields an excess in the positive area by as much as 15% (and a concomitant decrease in the negative area), will not result in a loss of persistence and memory.

Multi-dendrite computation

The local nature of calcium signaling enables the system to take advantage of the presence of multiple dendritic branches by using them to perform parallel computation (**Fig. 6a**). One advantage of parallel computation is the ability to overcome the adverse effects of heterogeneity and noise, which are abundant in biological systems. Multidendritic computation overcomes these effects in the same way as the pooling of noisy signals in neuronal ensembles. An example is

Figure 3 The conversion of $[Ca^{2+}]_i$ into spikes. (**a**) A schematic drawing of a model neuron composed of one dendritic process (blue, low $[Ca^{2+}]_i$; red, high $[Ca^{2+}]_i$). The conductance of calcium-dependent cationic channels depends on the local $[Ca^{2+}]_i$, and therefore the total calcium-dependent cationic current is proportional to the location of the front along the dendrite. (**b**) Simulation of the firing rate of the model neuron as a function of the location of the front along a 30-μm dendrite (see **Supplementary Methods** online).

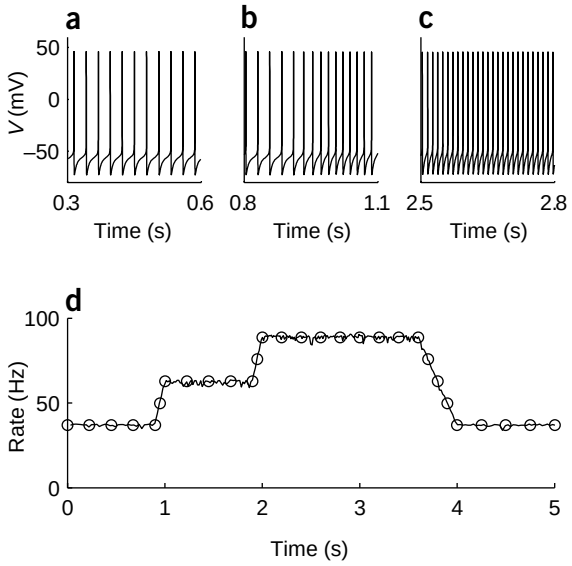

Figure 4 Integration of a time-dependent spatially homogeneous stimulus. The input is the same as in **Fig. 2a**, and the model neuron is as in **Fig. 3**. (**a**–**c**) The membrane potential at three time intervals, denoted by black bars in **Fig. 2a**. (**a**) Initially there is no synaptic input, and the firing rate persists at a constant rate, which corresponds to a stationary calcium front. (**b**) With the onset of the external input, the location of the front and consequently the firing rate change in proportion to the integral over time of the input. (**c**) After the termination of the input, the spiking activity shows a new persistent state, this time at a different rate, encoding the new position of the $[Ca^{2+}]_i$ front. (**d**) The instantaneous firing rate (the inverse of the interspike interval; line) is proportional to the location of the front and accurately reproduces the integral over time of the input (circles).

shown in **Fig. 6b–f**, where multiple branches integrate sinusoidal inputs, similar to time-varying head velocity in VOR experiments. Here, each granular dendrite receives the same cosine stimulus (**Fig. 6b**) in the presence of random spatial inhomogeneity in the dendritic calcium dynamics, that is, in the distribution of calcium stores or the synaptic inputs (equation (7) in Methods). Because of this spatial inhomogeneity, each dendrite shows a considerable drift in the location of the $[Ca^{2+}]_i$ front (**Fig. 6d**,**e**). Therefore, a firing rate based on the calcium dynamics in a single dendrite would significantly deviate from a perfect integrator. However, the total area of high $[Ca^{2+}]_i$ summed over 100 dendritic branches deviates only slightly from the desired integration, and therefore the firing rate of single neurons can accurately integrate incoming inputs even in the presence of strong noise (compare **Fig. 6c** and **f**).

DISCUSSION

Calcium computation

The nonlinear and local nature of calcium dynamics enables cells to generate a wide repertoire of spatiotemporal patterns, which are used to control processes as diverse as fertilization, proliferation and development, but also cell death through necrosis and apoptosis[17]. In neurons, calcium modulates membrane potential, synaptic release, short- and long-term plasticity and axonal growth[33]. Calcium is also critically involved in other information processing tasks, such as the detection of the direction of image motion in rabbit retina[34]. Very recently, graded persistent activity, which relies on activity-dependent $[Ca^{2+}]_i$ changes, has been found in single neurons in slices of entorhinal cortex[15]. This area is known to be associated with memory functions, and the established persistent activity has been proposed as a single-neuron mechanism subserving working memory. In this study, we have shown that calcium dynamics can also be the physiological basis for the graded persistent activity observed in neurons during temporal integration tasks.

We based our model on the hypothesis that calcium wave-fronts result from the combined effect of local calcium bistability and diffusion. This mechanism of wave- front generation by bistability and diffusion is quite general and has been studied extensively in many systems of excitable media[35]. In the present case, we propose that the bistability between two equilibria of calcium levels is the outcome of CICR. To generate the desired $[Ca^{2+}]_i$ bistability by CICR, several conditions must be met. It may be necessary to assume that the flux of calcium through the plasma depends on the concentration of calcium in the stores[36] or that this flux is small compared to the flux through the calcium stores membrane[26,27,37]. In addition, high levels of $[Ca^{2+}]_i$ have been shown to inactivate the release of calcium from internal stores which could potentially destabilize the high calcium state[38]. The slow oscillations and wave fronts of $[Ca^{2+}]_i$ observed in diverse biological systems[16–25] indicate in our view, that under diverse conditions this inactivation is only partial and therefore does not destroy $[Ca^{2+}]_i$ bistability[39]. Our work calls for experimental elucidation of the mechanisms underlying calcium bistability and wave-fronts in nerve cells.

The dynamic range of calcium concentration participating in calcium computation is still unclear, particularly as high calcium concentrations are toxic and can result in cell death. Several studies have shown that in darkness, the cytoplasmic calcium concentration in retinal rods is 0.25–0.55 μM[40–42]. Its concentration in suprachiasmatic neurons oscillates with a 24-h period, alternating between 0.44 μM at the circadian peak and 0.12 μM at the nadir[43]. These values are consistent with our model, in which the calcium concentration cannot exceed 0.4 μM.

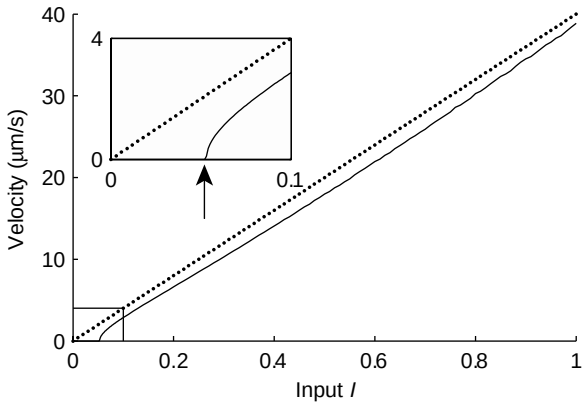

Figure 5 The velocity of the front as a function of the constant external input in a granular dendrite. Dotted line represents a continuous homogeneous dendrite; solid line shows a simulation of a granular dendrite (equation (7) in Methods), with 15 compartments of size $\Delta x = 2$ μm. Inset, magnification of the boxed region. Note that when the input is smaller than $I = 0.05$ (arrow), the front does not move, giving rise to an input threshold (see magnification in inset) However, the response to stronger inputs in the granular case is very similar to the response in the homogeneous, continuous dendrite.

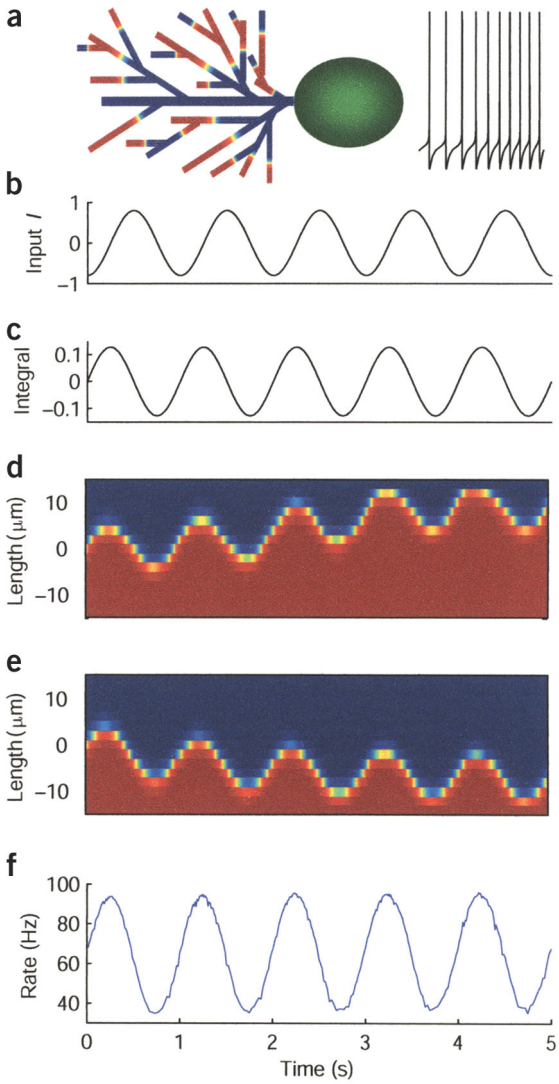

Figure 6 Parallel integration of input by multiple dendritic branches in the presence of noise. (**a**) A schematic drawing of the neuron. The entire dendritic tree receives the same time-dependent spatially homogeneous input, in addition to time-independent inhomogeneous noise. $[Ca^{2+}]_i$ fronts propagate along many different dendritic branches simultaneously, with velocities which depend on the homogeneous input, but also on the local noise in each branch (red, high $[Ca^{2+}]_i$; blue, low $[Ca^{2+}]_i$). The locations of the $[Ca^{2+}]_i$ fronts in all the dendritic branches determine the total amount of calcium-dependent current that reaches the axon hillock and consequently the firing rate. (**b**–**f**) An example of a simulation of dendritic integration of sinusoidal VOR input $I(t) = A\cos(\omega t)$, with $A = 0.8$, $\omega = 2\pi$ Hz, in the presence of strong quenched noise I_x which is sampled independently for each dendritic compartment of size $\Delta x = 2$ μm from a uniform distribution between –0.2 and 0.2 (Methods). (**b**) The homogeneous input. (**c**) The temporal integral of the input. (**d**,**e**) Location of $[Ca^{2+}]_i$ fronts as a function of time in two dendritic branches. Note that the main effect of the noise is the slow drift in the location of the front, which prevents accurate integration of the time-dependent input based on a single dendritic branch (compare to **c**). Color scale as in **Fig. 2**. (**f**) The total calcium concentration of a neuron with 100 dendritic branches averages out the spatial noise in the different branches, yielding a firing rate (blue) that accurately follows the temporal integral of the input (**c**).

Relation to previous work

Previous models of neural integrators have assumed that integration is the outcome of the collective behavior of recurrent excitatory networks. The early models approximated the neurons and the synaptic connections as linear elements[7–11]. Despite their lack of biophysical realism, these models provided a conceptual framework for understanding the conditions in which network interactions give rise to long time scales and enable accurate integration. Essentially, the long time scale, which is required for holding the value of a position variable in memory, is achieved by tuning the network connections such that the gain of the network is exactly 1. These models suffer from lack of robustness to small changes in the network parameters. For example, a slight increase in the overall coupling strength results in an increase in the network gain, leading to divergent neuronal activity. Conversely, a slight decrease in the coupling strength results in convergence to a single stable state and the loss of the memory of the desired integral. In addition, it was unclear how networks composed of spiking neurons could possess a constant gain at different levels of activity. These linear network models have been extended to incorporate conductance-based neurons with a highly nonlinear spiking mechanism and biologically feasible synapses[12]. The combination of a threshold-linear, frequency-current curve for single neurons and synaptic saturation gives rise to nearly constant network gain, which can be made to be close to 1 throughout the network dynamic range. The introduction of nonlinearity to the model also makes it more robust to small changes in the network parameters. However, the required level of fine-tuning of the parameters of the single-neuron dynamics and the synaptic strengths still remains high. Several learning rules have been proposed as possible mechanisms for self-tuning of the network connections to the desired values[44–46], but at present, the efficiency of these rules remains unclear. A different solution to the problem of robust integration has recently been proposed[13], which is based on embedding bistable neurons in a heterogeneous recurrent network. It has been shown that such a network can integrate incoming inputs robustly, even when the network parameters are not finely tuned. However, it is difficult to reconcile this model with the absence of bistability in the membrane potential of neurons of the goldfish oculomotor neuronal integrator[6]. The underlying assumption of the models mentioned above is that persistent activity and integration are an emergent property of recurrent network dynamics. However, accumulating experimental data suggest that at least in the goldfish oculomotor neuronal integrator, the observed behavior is the outcome of the properties of single neurons and does not rely on network interactions, supporting our hypothesis of a single-neuron integrator. The underlying nonlinearity and granularity of our model endows it with a considerable degree of robustness to global mistuning of parameters. In addition, robustness to local spatial inhomogeneity is provided by averaging over multiple dendritic branches.

Experimental predictions

Our model predicts that regenerative spatiotemporal patterns of $[Ca^{2+}]_i$ dynamics exist in the dendrites of neurons in prefrontal cortex, hippocampus and integrator brainstem nuclei, and that they vary systematically with synaptic input and sensory stimuli in a graded fashion. The existence of these patterns can be verified experimentally by calcium imaging techniques, and the pharmacological manipulation of intrinsic calcium dynamics would interfere with normal integration. Additionally, persistence and integration should be observed even in the absence of recurrent synaptic input. Such experiments may reveal that as a computational system, the single

neuron is far more powerful than the McCulloch and Pitts[47] point-like threshold unit that has dominated much of neural modeling in the past half-century.

METHODS

The autocatalytic $[Ca^{2+}]_i$ dynamics in one small dendritic compartment is described by a simple phenomenological model, a third order polynomial function:

$$\frac{dc}{dt} = f(c); f(c) \equiv -K(c-c_1)\cdot(c-c_2)\cdot(c-c_3) \quad (1)$$

where $c = [Ca^{2+}]_i$. The terms c_1 (0.1 μM) and c_3 (0.4 μM) correspond to the low and high $[Ca^{2+}]_i$ stable fixed points, respectively. The values of c_1 and c_3 are chosen such that the dynamics of $[Ca^{2+}]_i$ falls within the physiological range[17]. The c_2 value is the unstable intermediate fixed point ($c_1 < c_2 < c_3$). The value of K (889 $\mu M^{-2}s^{-1}$) is chosen so that the front width equals 2 μm (see below).

Incorporating the diffusion in a homogeneous dendrite, we obtain the one-dimensional reaction-diffusion equation:

$$\frac{\partial c}{\partial t} = f(c) + D\,\frac{\partial^2 c}{\partial x^2} \quad (2)$$

where D is the cytoplasmic calcium diffusion coefficient. The diffusion coefficient of free calcium in the cytoplasm is $D_{free} = 220\ \mu m^2 s^{-1}$, but its buffering strongly reduces the effective diffusion coefficient to $D_{eff} = 10$–$70\ \mu m^2 s^{-1}$, depending on its concentration[48]. Here we take $D = 40\ \mu m^2 s^{-1}$. We assume that one end of the dendrite, say the left end, is held at high $[Ca^{2+}]_i$ while the other end is held at low $[Ca^{2+}]_i$. The boundary conditions could result from heterogeneity at the ends of the dendrite. For example, deficiency of calcium stores at one end would result in low values of $[Ca^{2+}]_i$, whereas a high density of calcium channels will generate high local values of $[Ca^{2+}]_i$. The solution of the above reaction diffusion equation for a long dendrite[35] has the form of a front, which moves with constant velocity:

$$c(x,t) = \frac{c_1+c_3}{2} + \frac{c_3-c_1}{2}\tanh\left(\frac{x-L(t)}{\lambda}\right);\ \lambda = \frac{2\sqrt{2D}}{(c_3-c_1)\sqrt{K}} \quad (3)$$

where λ is the width of the front. With the above parameters, $\lambda = 2$ μm, similar to experimental observations[24]. The center of the front equals:

$$L(t) = L(0) + vt;\quad v = \sqrt{2DK}\,(c_2 - c_m);\quad c_m = \tfrac{1}{2}(c_3 + c_1) \quad (4)$$

where v is the front velocity. With our parameters, the maximum value of v is $S = 40$ μm/s. In the case where c_2 is half-way between c_1 and c_3 ($c_2 = c_m$), $v = 0$ and the front is stationary at a location $L(0)$, which can be anywhere in the bulk of the dendrite. We have chosen a cubic form for the reaction function $f(c)$ in equation (1) for its analytical tractability. The qualitative behavior of our model is insensitive to the precise form of this function. In general, the sign and magnitude of the front velocity depends on the area under the reaction function. This can be seen by a spatial integration of equation (2). Noting that the derivatives of the front profile near the boundaries are small, the net rate of change in calcium is proportional to the integral of $f(c)$. Hence if the negative and positive areas under $f(c)$ are equal the front is stationary[35].

We modeled the effect of a spatially homogeneous synaptic input on $[Ca^{2+}]_i$ by:

$$\frac{\partial c}{\partial t} = f(c) + D\,\frac{\partial^2 c}{\partial x^2} + g(c)\cdot I(t);\ \ g(c) \equiv K\cdot\frac{c_3-c_1}{2}\cdot(c-c_1)\cdot(c-c_3) \quad (5)$$

where $I(t)$ is the time-dependent and spatially independent input in dimensionless units between –1 and 1. The function $g(c)$ describes the $[Ca^{2+}]_i$ dependence of the response of the receptors and the stores to incoming input. When $c \approx c_1$ or $c \approx c_3$, $g(c) \approx 0$, preventing $[Ca^{2+}]_i$ from exceeding the saturation terms c_1 and c_3. Indeed, both low and high $[Ca^{2+}]_i$ block ionic channels[49,50]. In our model, $c_2 = c_m$, so that in the absence of input, the front is stationary at an arbitrary location. The effect of the input $I(t)$ is equivalent to changing the value of c_2. In fact, the solution of equation (5) is the same as equation (3), but with:

$$L(t) = S\cdot\int^t dt'\, I(t') \quad (6)$$

We modeled a granular dendrite as a one-dimensional chain of connected compartments positioned at locations x, which are multiples of Δx, where Δx is the length of each compartment. We can describe the $[Ca^{2+}]_i$ dynamics using the following set of differential equations:

$$\frac{dc_x}{dt} = f(c_x) + \frac{D}{\Delta x^2}\,(c_{x+\Delta x} - 2c_x + c_{x-\Delta x}) + g(c_x)\cdot I(t) \quad (7)$$

where c_x is $[Ca^{2+}]_i$ in the dendritic compartment located at x. Spatial noise is introduced by replacing $I(t)$ in equation (7) by $[I_x + I(t)]$, where I_x is a time-independent random noise to the compartment at x, drawn from a uniform distribution, independently for each compartment.

The spiking neuron parameters appear in the **Supplementary Methods** online.

Note: Supplementary information is available on the Nature Neuroscience website.

ACKNOWLEDGMENTS

We thank M. Goldman, D. Hansel, H.G. Rotstein, M. Spira and Y. Yarom for discussions. This work was supported in part by the Israeli Science Foundation (Center of Excellence 8006-00). Y.L. was supported by the Yeshaya Horowitz Association.

COMPETING INTERESTS STATEMENT

The authors declare that they have no competing financial interests.

Received 14 April; accepted 17 July 2003
Published online at http://www.nature.com/natureneuroscience/

1. Gnadt, J.W. & Andersen, R.A. Memory related motor planning activity in posterior parietal cortex of macaque. *Exp. Brain Res.* **70**, 216–220 (1988).
2. Funahashi, S., Bruce, C.J. & Goldman-Rakic, P.S. Mnemonic coding of visual space in the monkey's dorsolateral prefrontal cortex. *J. Neurophysiol.* **61**, 331–349 (1989).
3. Romo, R., Brody, C.D., Hernandez, A. & Lemus, L. Neuronal correlates of parametric working memory in the prefrontal cortex. *Nature* **399**, 470–473 (1999).
4. Compte, A., Brunel, N., Goldman-Rakic, P.S. & Wang, X.J. Synaptic mechanisms and network dynamics underlying spatial working memory in a cortical network model. *Cereb. Cortex* **10**, 910–923 (2000).
5. Aksay, E., Baker, R., Seung, H.S. & Tank, D.W. Anatomy and discharge properties of pre-motor neurons in the goldfish medulla that have eye-position signals during fixations. *J. Neurophysiol.* **84**, 1035–1049 (2000).
6. Aksay, E., Gamkrelidze, G., Seung, H.S., Baker, R. & Tank, D.W. *In vivo* intracellular recording and perturbation of persistent activity in a neural integrator. *Nat. Neurosci.* **4**, 184–193 (2001).
7. Rosen, M.J. A theoretical neural integrator. *IEEE Trans. Biomed. Eng.* **19**, 362–367 (1972).
8. Cannon, S.C., Robinson, D.A. & Shamma, S. A proposed neural network for the integrator of the oculomotor system. *Biol. Cybern.* **49**, 127–136 (1983).
9. Galiana, H.L. & Outerbridge, J.S. A bilateral model for central neural pathways in vestibuloocular reflex. *J. Neurophysiol.* **51**, 210–241 (1984).
10. Seung, H.S. How the brain keeps the eyes still. *Proc. Natl. Acad. Sci. USA* **93**, 13339–13344 (1996).
11. Arnold, D.B. & Robinson, D.A. The oculomotor integrator: testing of a neural network model. *Exp. Brain Res.* **113**, 57–74 (1997).
12. Seung, H.S., Lee, D.D., Reis, B.Y. & Tank, D.W. Stability of the memory of eye position in a recurrent network of conductance-based model neurons. *Neuron* **26**, 259–271 (2000).
13. Koulakov, A.A., Raghavachari, S., Kepecs, A. & Lisman, J.E. Model for a robust neural integrator. *Nat. Neurosci.* **5**, 775–782 (2002).
14. Pastor, A.M., De la Cruz, R.R. & Baker, R. Eye position and eye velocity integrators reside in separate brainstem nuclei. *Proc. Natl. Acad. Sci. USA* **91**, 807–811 (1994).

15. Egorov, A.V., Hamam, B.N., Fransen, E., Hasselmo, M.E. & Alonso, A.A. Graded persistent activity in entorhinal cortex neurons. *Nature* **420**, 173–178 (2002).
16. Goldbeter, A., Dupont, G. & Berridge, M.J. Minimal model for signal-induced Ca^{2+} oscillations and for their frequency encoding through protein phosphorylation. *Proc. Natl. Acad. Sci. USA* **87**, 1461–1465 (1990).
17. Berridge, M.J., Lipp, P. & Bootman, M.D. The versatility and universality of calcium signalling. *Nat. Rev. Mol. Cell Biol.* **1**, 11–21 (2000).
18. Finch, E.A. & Augustine, G.J. Local calcium signalling by inositol-1,4,5-trisphosphate in Purkinje cell dendrites. *Nature* **396**, 753–756 (1998).
19. Nakamura, T. *et al*. Inositol 1,4,5-trisphosphate (IP3)-mediated Ca^{2+} release evoked by metabotropic agonists and backpropagating action potentials in hippocampal CA1 pyramidal neurons. *J. Neurosci.* **20**, 8365–8376 (2000).
20. Charles, A.C., Merrill, J.E., Dirksen, E.R. & Sanderson, M.J. Intercellular signaling in glial cells: calcium waves and oscillations in response to mechanical stimulation and glutamate. *Neuron* **6**, 983–992 (1991).
21. Finkbeiner, S. Calcium waves in astrocytes-filling in the gaps. *Neuron* **8**, 1101–1108 (1992).
22. Sneyd, J., Keizer, J. & Sanderson, M.J. Mechanisms of calcium oscillations and waves: a quantitative analysis. *Faseb J.* **9**, 1463–1472 (1995).
23. Fontanilla, R.A. & Nuccitelli, R. Characterization of the sperm-induced calcium wave in *Xenopus* eggs using confocal microscopy. *Biophys. J.* **75**, 2079–2087 (1998).
24. Wolszon, L.R., Rehder, V., Kater, S.B. & Macagno, E.R. Calcium wave fronts that cross gap junctions may signal neuronal death during development. *J. Neurosci.* **14**, 3437–3448 (1994).
25. Feller, M.B., Wellis, D.P., Stellwagen, D., Werblin, F.S. & Shatz, C.J. Requirement for cholinergic synaptic transmission in the propagation of spontaneous retinal waves. *Science* **272**, 1182–1187 (1996).
26. Sneyd, J. & Sherratt, J. On the propagation of calcium waves in an inhomogeneous medium. *SIAM J. Appl. Math.* **57**, 73–94 (1997).
27. Li, Y.X. & Rinzel, J. Equations for InsP3 receptor-mediated $[Ca^{2+}]i$ oscillations derived from a detailed kinetic model: a Hodgkin-Huxley like formalism. *J. Theor. Biol.* **166**, 461–473 (1994).
28. Kato, B.M. & Rubel, E.W. Glutamate regulates IP3-type and CICR stores in the avian cochlear nucleus. *J. Neurophysiol.* **81**, 1587–1596 (1999).
29. du Lac, S. & Lisberger, S.G. Membrane and firing properties of avian medial vestibular nucleus neurons *in vitro*. *J. Comp. Physiol. [A]* **176**, 641–651 (1995).
30. Serafin, M., de Waele, C., Khateb, A., Vidal, P.P. & Muhlethaler, M. Medial vestibular nucleus in the guinea-pig. I. Intrinsic membrane properties in brainstem slices. *Exp. Brain Res.* **84**, 417–425 (1991).
31. Shriki, O., Hansel, D. & Sompolinsky, H. Rate models for conductance based cortical neuronal networks. *Neural Comput.* **15**, 1809–1841 (2003).
32. Keener, J.P. Homogenization and propagation in the bistable equation. *Physica. D.* **136**, 1–17 (2000).
33. Kandel, E.R., Schwartz, J.H. & Jessell, T.M. (eds.) *Principles of Neural Science* (McGraw-Hill, New–York, 2000).
34. Euler, T., Detwiler, P.B. & Denk, W. Directionally selective calcium signals in dendrites of starburst amacrine cells. *Nature* **418**, 845–852 (2002).
35. Mikhailov, A.S. Foundation of Synergetics: Distributed Active Systems (Springer-Verlag,–Berlin, 1994).
36. Torres, J.J., Willems, P.H.G.M., Kappen, H.J. & Koopman, W.J.H. Hysteresis and bistability in a realistic model for IP3-driven Ca^{2+} oscillations. *Europhys. Lett.* **55**, 746–752 (2001).
37. De Young, G.W. & Keizer, J. A single-pool inositol 1,4,5-trisphosphate-receptor-based model for agonist-stimulated oscillations in Ca^{2+} concentration. *Proc. Natl. Acad. Sci. USA* **89**, 9895–9899 (1992).
38. Kupferman, R., Mitra, P.P., Hohenberg, P.C. & Wang, S.-H. Analytical calculation of intracellular calcium wave charachteristics. *Biophys. J.* **72**, 2430–2444 (1997).
39. Wagner, J., Li, Y.-X., Pearson, J. & Keizer, J. Simulation of the fertilization Ca^{2+} wave in xenopus laevis eggs. *Biophys. J.* **75**, 2088–2097 (1998).
40. Gray-Keller, M.P. & Detwiler, P.B. The calcium feedback signal in the phototransduction cascade of vertebrate rods. *Neuron* **13**, 849–861 (1994).
41. Lagnado, L., Cervetto, L. & McNaughton, P.A. Calcium homeostasis in the outer segments of retinal rods from the tiger salamander. *J. Physiol.* **455**, 111–142 (1992).
42. Woodruff, M.L. *et al*. Measurement of cytoplasmic calcium concentration in the rods of wild-type and transducin knock-out mice. *J. Physiol.* **542**, 843–854 (2002).
43. Ikeda, M. *et al*. Circadian dynamics of cytosolic and nuclear Ca^{2+} in single suprachiasmatic nucleus neurons. *Neuron* **38**, 253–263 (2003).
44. Arnold, D.B. & Robinson, D.A. A learning network model of the neural integrator of the oculomotor system. *Biol. Cybern.* **64**, 447–454 (1991).
45. Arnold, D.B. & Robinson, D.A. A neural network model of the vestibulo-ocular reflex using a local synaptic learning rule. *Philos. Trans. R. Soc. Lond. B Biol. Sci.* **337**, 327–330 (1992).
46. Xie, X. & Seung, H.S. Spike-based learning rules and stabilization of persistent neural activity. *Adv. Neural Inf. Process. Syst.* **12**, 199–205 (2000).
47. McCulloch, W.S. & Pitts, W.H. A logical calculus of the ideas immanent in nervous activity. *Bull. Math. Biophys* **5**, 115–133 (1943).
48. Allbritton, N.L., Meyer, T. & Lubert, S. Range of messenger action on calcium ion and inositol 1, 4, 5-trisphosphate. *Science* **258**, 1812–1815 (1992).
49. Perrier, J.F. & Hounsgaard, J. Ca^{2+}-activated nonselective cationic current (I(CAN)) in turtle motoneurons. *J. Neurophysiol.* **82**, 730–735 (1999).
50. Peterson, B.Z., DeMaria, C.D., Adelman, J.P. & Yue, D.T. Calmodulin is the Ca^{2+} sensor for Ca^{2+}-dependent inactivation of L-type calcium channels. *Neuron* **22**, 549–558 (1999).